

NKS-467
ISBN 978-87-7893-562-5

Effect of Thermal Ageing and Microstructure on Fracture Mechanical Behaviour of Ni-based Alloy Dissimilar Metal Welds

Zaiqing Que¹
Sebastian Lindqvist¹
Noora Hytönen¹
Yanling Ge¹
Kristina Lindgren²
Mattias Thuvander²
Pål Efsing^{3, 4}

¹ VTT Technical Research Centre of Finland Ltd, PO Box 1000
FI-02044 VTT, Espoo, Finland

² Chalmers University of Technology, Department of Physics
SE-412 96, Göteborg, Sweden

³ Ringhals AB, SE-43285 Väröbacka, Sweden

⁴ Department of Solid Mechanics, Royal Institute of Technology (KTH),
SE-100 44 Stockholm, Sweden

February 2023

Abstract

DMWs are commonly used to join austenitic and ferritic components in the RCPB and can become potential concerns regarding the structural integrity of the nuclear power SSC. In particular, the knowledge on the local strength mismatch at the LAS/nickel-based alloy weld metal interface upon PWHT and during long-term ageing is lacking. The amount of information available in the open literature on the fracture mechanical and microstructural changes occurring at the fusion boundary after buttering, welding, PWHT and long-term ageing is relative limited and often very case dependent. Understanding the fracture mechanical and microstructural appearance, behaviour and development of the complex DMW fusion boundary is crucial for both the improvement of nuclear component integrity and to ensure safe long-term operation. In this study, a Ringhals SA508/Alloy52 DMW mock-up consisting of Alloy 52 buttering on both sides (representative of Ringhals 3 pressurizer surge nozzle DMW) and a TVO NG DMW mock-up are studied, thus the test materials are representative of actual power plant components. The project promotes the knowledge transfer, improve the nuclear materials and fracture mechanics competence and strengthen the connections and experience exchange between the Nordic research organizations, universities, industries, authorities, and especially the young generation. The project deals with the structural integrity, long-term operation, and ageing management, which are relevant for both present and future nuclear power plants. The technical results provide a basis for assessment of long-term operation for the Finnish and Swedish nuclear power plants for both the operators and the regulatory perspectives. Dissemination through the open seminar, the peer reviewed publications and the oral presentations at the international conferences ensured the knowledge exchange in international and Nordic networks.

Key words

Dissimilar metal weld, Alloy 52, fusion boundary, characterisation, fracture mechanical test

NKS-467
ISBN 978-87-7893-562-5
Electronic report, February 2023
NKS Secretariat
P.O. Box 49
DK - 4000 Roskilde, Denmark
Phone +45 4677 4041
www.nks.org
e-mail nks@nks.org

Effect of Thermal Ageing and Microstructure on Fracture Mechanical Behaviour of Ni-based Alloy Dissimilar Metal Welds

Final Report from the NKS-R FEMMA activity (Contract: AFT/NKS-R(22)134/4)

Zaiqing Que¹, Sebastian Lindqvist¹, Noora Hytönen¹, Yanling Ge¹
Kristina Lindgren², Mattias Thuvander²
Pål Efsing^{3,4}

¹ VTT Technical Research Centre of Finland Ltd, PO Box 1000, FI-02044 VTT, Espoo, Finland

² Chalmers University of Technology, Department of Physics, SE-412 96, Göteborg, Sweden

³ Ringhals AB, SE-43285 Väröbacka, Sweden

⁴ Department of Solid Mechanics, Royal Institute of Technology (KTH), SE-100 44 Stockholm, Sweden

Table of contents

	Page
1. Introduction	3
2. Microstructural investigations on FBs of DMWs	4
3. Fracture mechanical tests on DMWs	5
4. Microstructural assessment using APT	6
5. Conclusions	7
6. References	7

1. Introduction

Dissimilar metal welds (DMWs) are commonly used to join austenitic and ferritic components in the reactor coolant pressure boundary, often using a nickel-based filler metal. DMWs can become potential concerns regarding the structural integrity of the nuclear power systems, structures and components. In particular, the knowledge on the local strength mismatch at the low alloy steel (LAS)/nickel-based alloy weld metal interface upon post-weld heat treatment (PWHT) and during long-term ageing is lacking. The amount of information available in the literature on the fracture mechanical and microstructural changes occurring at the fusion boundary (FB) after buttering, welding, PWHT and long-term ageing is relatively limited and often very case dependent. As a part of the NKS-R program in 2022, VTT, Chalmers University of Technology, and KTH have studied the microstructural properties and fracture mechanical performance of Alloy 52 narrow-gap (NG) DMW provided by TVO and Alloy 52 DMW mock-up consisting of Alloy 52 buttering on both sides provided by Ringhals in the FEMMA project.

The project dealt with the structural integrity, long-term operation, and ageing management, which are relevant for both present and future nuclear power plants. The technical results provide a basis for the assessment of long-term operation for the Finnish and Swedish nuclear power plants for both the operators and the regulatory perspectives. In 2022, the main progress has been in the area of mechanical testing and microstructural characterization of the DMW mock-ups.

A seminar, summarising the gained knowledge and lessons learned from the earlier DMW projects was arranged at KTH in September 2022 to facilitate spreading of the gained knowledge to the industry, authorities and research community, especially the young generation. The Finnish and Swedish nuclear operators, research organizations and regulatory bodies including Ringhals, Forsmark, OKG, KTH, Chalmers, TVO, VTT, Aalto University and STUK were actively involved in the discussions during the seminar.

The work was executed by young researchers including Noora Hytönen and Laura Sirkiä and young scientists Kristina Lindgren (Chalmers), Zaiqing Que (VTT) and Sebastian Lindqvist (VTT). Additionally, young researchers Pentti Arffman and Jari Lydman at VTT was integral part of the work.

2. Microstructural investigations on FBs of DMWs

The microstructural investigations were performed at the LAS/nickel-based alloy weld metal interface. High-magnification microstructural characterization by means of scanning electron microscopy (SEM)/ electron backscatter diffraction (EBSD), focused ion beam (FIB), wide-angle X-ray scattering (WAXS) and transmission electron microscopy (TEM) were performed at the FB region at VTT. The effect of thermal ageing on the carbon enrichment, and the evolution of the local mismatch during the aging were evaluated. In addition, the characteristics of the precipitates and other possible particles that have an effect on the initiation of brittle fracture were examined. Strength mismatch of the SA508/nickel-based Alloy 52 fusion interface was investigated by micro-hardness and nanoindentation measurements.

The microstructural characterization of the FB region shows mild differences, e.g. carbon diffusion and hardness, between the two DMW mock-ups due to the welding technique, welding orientation, thermal histories and thermal ageing. The fracture toughness testing indicates marginally better results for the DMW with buttering in reference condition, and no clear thermal ageing effect is observed in the NG DMW fracture toughness.

The metallographic microstructure and FBs were studied. In the NG mock-up, the majority of the FB is a narrow and straight boundary between SA508 and A52. Few large swirls with partial mixed zones were observed correlating with the weld bead solidification structure, where also type-II boundaries were found on the weld side. In the buttering mock-up, the FB is mostly narrow and straight but additionally tempered martensitic transition zones and partial mixed zones were locally observed. No significant swirls or type-II boundaries were found, which is due to the different welding orientation affecting the weld pool mixing.

Microhardness measurements of HV1 and HV0.3 reveal a hardness peak at the LAS heat affected zone in both weld mock-ups, although in the buttering DMW, the peak is higher and the overall hardness level is ~20 HV higher (as shown in Figure 1). In the NG mock-up, the HV0.3 revealed a soft zone next to the heat affected zone hardness peak.

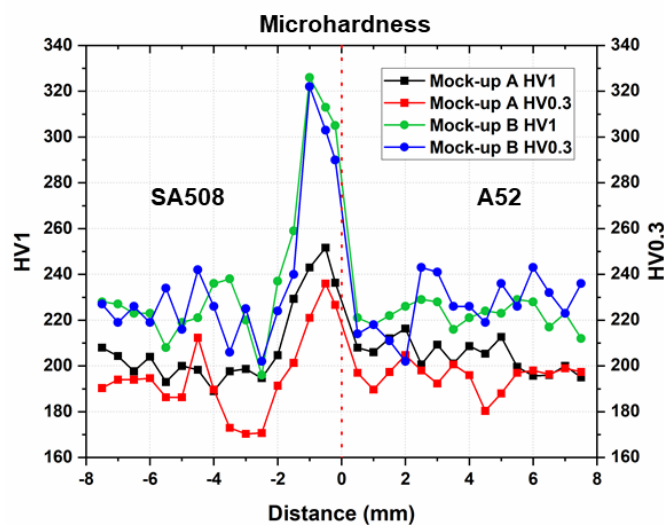


Figure 1: Microhardness across the FB of the two mock-ups. (A: NG mock-up; B: buttering mock-up)

The nanoindentations reveal local nano-hardness mismatch at the FB. The nano-hardness peak was observed in the A52 in the NG mock-up, and at the tempered martensite FB in the LAS in the buttering mock-up. The partial mixed zone in the buttering mock-up did not show an evident peak.

The carbide analysis in the heat affected zone using TEM revealed that in the NG mock-up the larger carbides are $(Fe, Mn, Cr)_3C$ with higher Mn content than Cr. Small carbides are mainly Mo_2C carbides although Cr-rich carbides were observed sparsely. In the buttering mock-up, the larger carbides are $(Fe, Mn, Cr)_3C$ with equal content of Mn and Cr. The small carbides were identified as Mo_2C .

To sum up, the microstructural characteristics of the two different mock-up types, with and without buttering, shows some differences at the LAS/nickel-based alloy weld metal interface microstructures and this gives important input when analysing and understanding the mechanical behaviour of the DMWs also after long-term operation.

3. Fracture mechanical tests on DMWs

The fracture mechanical tests were performed at VTT for both NG and buttering DMWs. The fracture properties were characterized according to ASTM E1921 to obtain the transition temperature T_0 and EN ISO 148-1 to obtain T_{28J} and T_{41J} . The impact toughness testing was done using an instrumented impact hammer to obtain the arrest force and arrest toughness. The crack was nominally placed at the FB between the weld metal and the LAS. The fracture toughness and impact toughness data are shown in Figure 2.

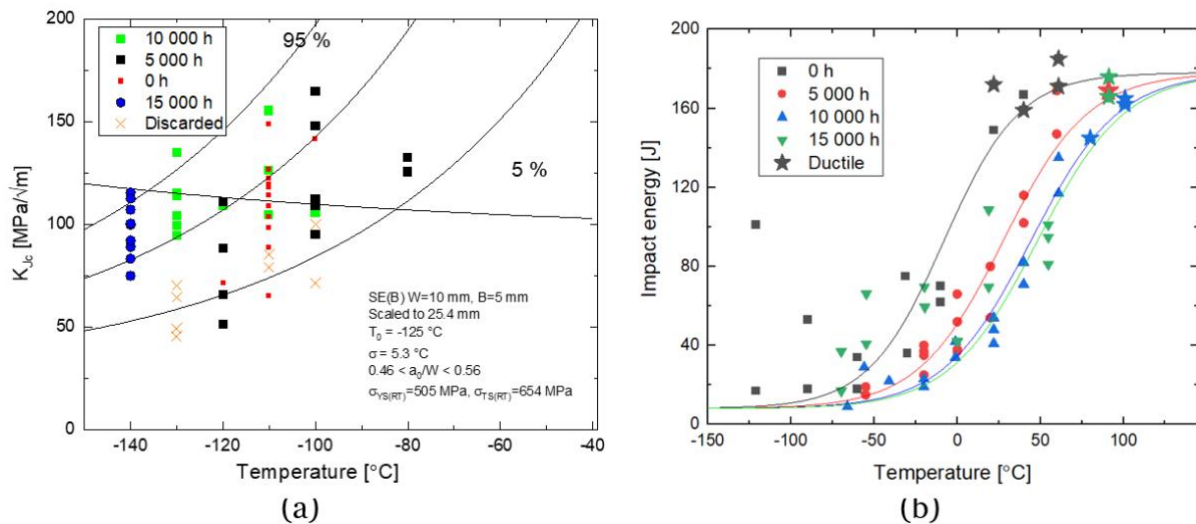


Figure 2. (a) T_0 results with the crack path deviating towards the fusion boundary; (b) Transition curves of impact energies for reference, 5 000 h, 10 000 h and 15 000 h aged conditions. The star symbols indicate 100 % ductile fracture.

The initiation of brittle fracture tends to occur next to the FB in the carbon-depleted zone. For cracks farther from the fusion boundary, in the HAZ, the crack deviates to the FB and progresses in that region, in most cases.

The effect of aging on the shift in impact toughness appears to saturate after 10 000 h of thermal aging. T_0 testing results in a lower shift than impact toughness testing. The crack location corrected T_0 shift is 10 °C after 15 000 h at 400 °C, whereas ΔT_{28J} is 49 °C. The

ΔT_{28J} and ΔT_{41J} saturate after 10 000 h at 400 °C, while ΔT_0 appears to saturate after 5 000 h. The T_0 for the NG DMW after 15 000 h of aging at 400 °C is of the same magnitude as after 10 000 h, 5 000 h and in AR references condition, as long as the crack is close enough to the FB. For cracks farther away, the fracture toughness appears to be lower.

The different shifts from the impact toughness and fracture toughness testing can be explained by the nature of the test methods. The fracture toughness describes the stress intensity required to initiate brittle fracture in the DBTT region, whereas the impact toughness describes the energy required to initiate, propagate and arrest a crack. Additionally, the fracture toughness specimens are more sensitive for the crack/notch location relative to the FB in the HAZ compared to impact toughness specimens since the fracture process zone of an impact toughness specimen samples a larger region.

The thermal aging mechanism can affect more the crack arrest and propagation mechanism than the initiation mechanism. The crack arrest toughness temperature increases with 35 °C after 15 000 h at 400 °C.

4. Microstructural assessment using APT

Atom probe tomography (APT) measurements at Chalmers University of Technology was used to identify the elemental segregation (especially phosphorous) at the boundaries upon ageing, primarily by comparing the phosphorous content of interiors of the grains and comparing the non-aged condition to the thermally-aged condition of the NG mock-up. In Figure 3, representative reconstructions of non-aged condition and thermally-aged condition are shown.

The phosphorous contents are 50 ± 20 at.ppm and 40 ± 20 at.ppm in the non-aged condition and thermally-aged condition, respectively. Though the bulk phosphorous content in the interior of the HAZ grains are slightly lower in the thermally-aged condition than in the non-aged condition material, there is no evidence of a significant phosphorous segregation to grain boundaries from thermal aging.

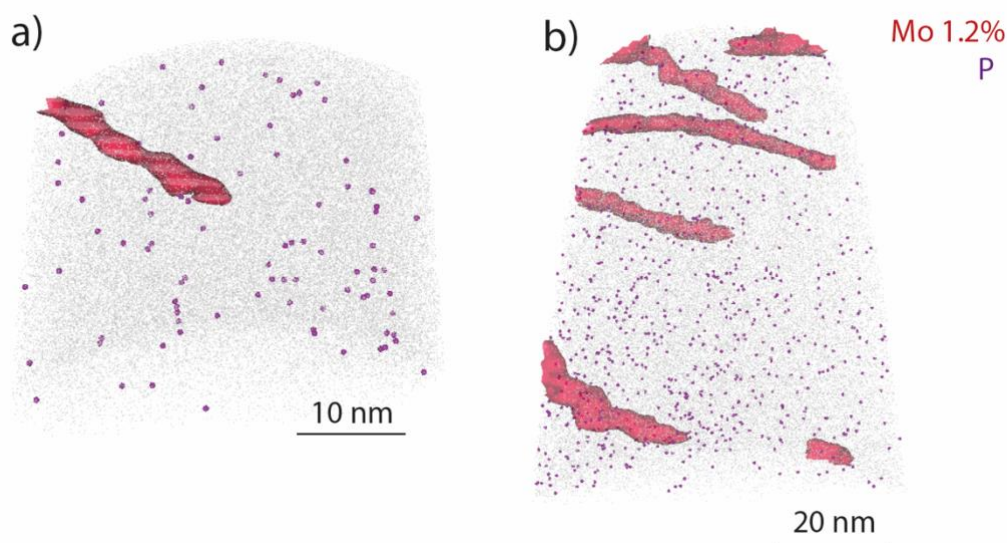


Figure 3. (a) APT reconstructions of (a) non-aged condition and (b) thermally-aged condition of the NG mock-up. The red features show Mo segregation to dislocations.

5. Conclusions

The microstructure and carbides in the fusion boundary (FB) and low alloy steel (LAS) heat-affected zone (HAZ) were analysed for the narrow-gap (NG) SA508/Alloy 52 dissimilar metal weld (DMW) mock-up and the DMW mock-up consisting of Alloy 52 buttering on both sides. Moderate differences at the LAS/nickel-based alloy weld metal interface microstructures of these two DMWs are found in the hardness and carbide types. There is no evidence of a significant phosphorus segregation to grain boundaries in HAZ due to thermal ageing, based on the APT measurements.

The fracture toughness testing indicates marginally better results for the DMW with buttering in reference condition, and no clear thermal ageing effect is observed in the NG DMW fracture toughness. The thermal ageing mechanism can affect more the crack arrest and propagation mechanism than the crack initiation mechanism.

6. References

- S. Lindqvist, Z. Que, P. Nevasmaa and N. Hytönen, “The effect of thermal aging on fracture properties of a narrow-gap Alloy 52 dissimilar metal weld,” *Engineering Fracture Mechanics*, 2023, DOI: 10.1016/j.engfracmech.2023.109056.
- Y. Ge, Z. Que, K. Lindgren, N. Hytönen, M. Thuvander, “Effect of Thermal Aging on Microstructure and Carbides of SA508/Alloy 52 Dissimilar Metal Weld,” submitted to *Materials Characterization*, 2023
- N. Hytönen, Y. Ge, Z. Que, S. Lindqvist, P. Nevasmaa, I. Virkkunen and P. Efsing, “Study of Fusion Boundary Microstructure and Local Mismatch of SA508/Alloy 52 Dissimilar Metal Weld,” submitted to *Journal of Nuclear Materials*, 2023.
- Lindqvist, S., Hytönen, N., Sirkiä, L., Arffman, P., Lydman, J., Ge, Y., Nevasmaa, P. & Que, Z., “Fracture in the Ductile-To-Brittle Transition Region of A Narrow-Gap Alloy 52 and Alloy 52 Dissimilar Metal Weld With Buttering,” *ASME PVP*, Nov 2022, doi: 10.1115/PVP2022-80690.
- N. Hytönen, Y. Ge, Z. Que, S. Lindqvist, J. Lydman, U. Ehrnstén, P. Rautala, I. Virkkunen and P. Efsing, “Effect of Microstructure on Mechanical Behaviour of Ni-base Alloy Dissimilar Metal Welds,” *The 20th International Conference on Environmental Degradation of Materials in Nuclear Power Systems-Water Reactor meeting*, ED2021-17104. 2022, Colorado, USA.
- N. Hytönen, Z. Que, S. Lindqvist, J. Lydman, Y. Ge, I. Virkkunen, U. Ehrnstén, P. Rautala, P. Efsing, B. Forssgren, *Fusion Boundary Microstructure and Fracture Behaviour of a narrow-gap Alloy 52 Dissimilar Metal Weld and an Alloy 52 Dissimilar Metal Weld with Buttering*, *International Symposium Contribution of Materials Investigations and Operating Experience to LWRs’ Safety, Performance and Reliability*, FONTEVRAUD 10, September 2022, Avignon, France.

Acknowledgements

NKS conveys its gratitude to all organizations and persons who by means of financial support or contributions in kind have made the work presented in this report possible.

The authors wish to express their gratitude for the funding and support from Ringhals AB, OKG AB, Teollisuuden Voima Oyj and VTT Technical Research Centre of Finland within the FEMMA (Forum for the Effect of Thermal Ageing and Microstructure on Mechanical and EAC Behaviour of Ni-based Alloy Dissimilar Metal Welds) research project. The authors also thank NKS for funding the NKS-FEMMA (AFT/NKS-R(22)134/4) project. The authors would like to thank P. Arffman, J. Lydman, A. Nurmela and L. Sirkiä for the experimental contributions. The authors would like to thank U. Ehrnstén, B. Forssgren, H. Reinwall and H. Hänninen for suggestions and discussions.

Disclaimer

The views expressed in this document remain the responsibility of the author(s) and do not necessarily reflect those of NKS. In particular, neither NKS nor any other organisation or body supporting NKS activities can be held responsible for the material presented in this report.

Title	Effect of Thermal Ageing and Microstructure on Fracture Mechanical Behaviour of Ni-based Alloy Dissimilar Metal Welds
Author(s)	Zaiqing Que ¹ , Sebastian Lindqvist ¹ , Noora Hytönen ¹ , Yanling Ge ¹ Kristina Lindgren ² , Mattias Thuvander ² Pål Efsing ^{3,4}
Affiliation(s)	¹ VTT Technical Research Centre of Finland Ltd, PO Box 1000, FI-02044 VTT, Espoo, Finland ² Chalmers University of Technology, Department of Physics, SE-412 96, Göteborg, Sweden ³ Ringhals AB, SE-43285 Väröbacka, Sweden ⁴ Department of Solid Mechanics, Royal Institute of Technology (KTH), SE-100 44 Stockholm, Sweden
ISBN	978-87-7893-562-5
Date	February 2023
Project	NKS-R FEMMA activity (Contract: AFT/NKS-R(22)134/4)
No. of pages	10
No. of tables	0
No. of illustrations	2
No. of references	6
Abstract max. 2000 characters	DMWs are commonly used to join austenitic and ferritic components in the RCPB and can become potential concerns regarding the structural integrity of the nuclear power SSC. In particular, the knowledge on the local strength mismatch at the LAS/nickel-based alloy weld metal interface upon PWHT and during long-term ageing is lacking. The amount of information available in the open literature on the fracture mechanical and microstructural changes occurring at the fusion boundary after buttering, welding, PWHT and long-term ageing is relative limited and often very case dependent. Understanding the fracture mechanical and microstructural appearance, behaviour and development of the complex DMW fusion boundary is crucial for both the improvement of nuclear component integrity and to ensure safe long-term operation. In this study, a Ringhals SA508/Alloy52 DMW mock-up consisting of Alloy 52 buttering on both sides (representative of Ringhals 3 pressurizer surge nozzle DMW) and a TVO NG DMW mock-up are studied, thus the test materials are representative of actual power plant components. The project promotes the knowledge transfer, improve the nuclear materials and fracture mechanics competence and strengthen the connections and experience exchange between the Nordic research organizations, universities, industries, authorities, and especially the young generation. The project deals with the structural integrity, long-term operation, and ageing management, which are relevant for both present and future

nuclear power plants. The technical results provide a basis for assessment of long-term operation for the Finnish and Swedish nuclear power plants for both the operators and the regulatory perspectives. Dissemination through the open seminar, the peer reviewed publications and the oral presentations at the international conferences ensured the knowledge exchange in international and Nordic networks.

Key words

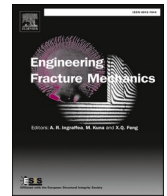
Dissimilar metal weld, Alloy 52, fusion boundary, characterisation, fracture mechanical test



ELSEVIER

Contents lists available at ScienceDirect

Engineering Fracture Mechanics

journal homepage: www.elsevier.com/locate/engfracmech

The effect of thermal aging on fracture properties of a narrow-gap Alloy 52 dissimilar metal weld

Sebastian Lindqvist^{*}, Zaiqing Que, Pekka Nevasmaa, Noora Hytönen

VTT, Kemistintie 3, Espoo 02660, Finland

ARTICLE INFO

Keywords:

Fracture toughness
T₀
Arrest toughness
DMW
Thermal aging

ABSTRACT

In nuclear power plants, dissimilar metal welds belong to safety class 1. The effect of thermal aging at 400 °C up to 15 000 h on ductile-to-brittle transition (DBT) region was investigated for an Alloy 52 dissimilar metal weld (DMW). The cracks and the notches were placed close to the fusion boundary between the low-alloy steel (LAS) and the weld metal. In previous work for DMWs, the shifts in different DBT temperatures have not been investigated, including reference temperature T₀, impact toughness-based T_{28J} and reference temperature for arrest toughness, T_{KIa}. The results show that the T₀ reference temperature does not change significantly with aging time, only 10 °C, but the shift in T_{28J} is 49 °C after 15 000 h. The shift in T_{KIa} is 35 °C. The results indicate that the aging mechanism affects more the crack propagation and arrest properties than brittle fracture initiation.

1. Introduction

In nuclear power plants (NPP), the reactor pressure vessel and pressurizer are made of low-alloy steel (LAS) and the pipes are made of austenitic stainless steel. The connecting welds are made of nickel-base alloys, and together they form a dissimilar metal weld (DMW). DMWs are safety critical components, and in operation, DMWs have been subjected to intergranular stress corrosion cracking (IGSCC) [1–3]. To address these challenges, the materials and manufacturing techniques have been improved, and today, narrow-gap (NG) Alloy 52 DMWs are used in modern European pressurized water reactors (EPR). The DMWs located in the outlet pipe of the reactor pressure vessel are subjected to a temperature of 330 °C that increases the susceptibility to thermal embrittlement. In the pressurizer, the temperature can be up to 350 °C. [4–6].

Most of the thermal aging data for Mn-Mo-Ni LASs (like SA 508, A533, 18MND5 and 16MND5) indicates that the materials are resistant to thermal aging in the temperature range of 260–320 °C for an aging time of 100 000 h and even up to 250 000 h. However, for few LASs, a shift of 60 °C in ductile-to-brittle transition temperature (DBTT) was reported [5]. In these cases, the alloys were not given a proper post-weld heat treatment (PWHT) or quench-and-temper heat treatment, or the reference and aged materials were sampled from different depths in thickness direction. These exceptions underline the need to investigate and understand the effects related to thermal aging.

An exceptionally high P or Ni content can result in a significant shift in DBTT due to thermal aging. Ni can affect the grain boundary absorption capacity of P atoms and increase the sensitivity to thermal embrittlement [7]. The DBTT shifted with 150 °C for a Mn-Mo-Ni LAS containing 1.7 % Ni, after aging at 330 °C for 20 000 h. VVER-1000 forgings and weld metals, Cr-Ni-Mo LASs, with Ni > 1.3 %,

^{*} Corresponding author.

E-mail address: Sebastian.lindqvist@vtt.fi (S. Lindqvist).

<https://doi.org/10.1016/j.engfracmech.2023.109056>

Received 6 October 2022; Received in revised form 21 December 2022; Accepted 4 January 2023

Available online 14 January 2023

0013-7944/© 2023 The Author(s).

Published by Elsevier Ltd.

This is an open access article under the CC BY license

(<http://creativecommons.org/licenses/by/4.0/>).

Nomenclature

A	Fitting parameter
ASTM	American society for testing and materials
B	Thickness
BM	Base metal
CDZ	Carbon depleted zone
CMOD	Crack-mouth opening displacement
C(T)	Compact tension
CVN	Charpy-V notch
DBTT	Ductile-to-brittle transition temperature
DMW	Dissimilar metal weld
EDWC	Electro-discharge wire cutter
F _a	Arrest force
F _m	Maximum force
F _u	Initiation force
GTAW	Gas tungsten arc welding
HAZ	Heat-affected zone
IGSCC	Inter-granular stress corrosion cracking
ISO	International organization for standardization
K _{Jc,limit}	Maximum K _{Jc} capacity
L	Length
LAS	Low alloy steel
NG	Narrow-gap
NPP	Nuclear power plant
PWHT	Post-weld heat treatment
SE(B)	Single edge bend
SEM	Scanning electron microscopy
SS	Stainless steel
T ₀	Master curve reference temperature
T _{28J}	CVN 28 J transition temperature
T _{41J}	CVN 41 J transition temperature
T _{fa4}	Reference temperature for arrest force
T _{KIa}	Crack arrest reference temperature
USE	Upper-shelf energy
WM	Weld metal
W	Width
σ	Standard deviation

show shifts up to 30 °C after thermal aging at 310–320 °C for 200 000 h. [5,6,8,9] The effect of Ni on the aging behavior has been connected to synergetic effects with other elements, e.g. Mn. [10–12].

P segregation to the grain boundaries is considered to be the main thermal aging mechanism for LAS in NPPs. Therefore, the P content has been restricted to 0.015 % and later to 0.008 % [4]. Thermal aging of LAS in NPPs is to a minor extent affected by segregation of other interfacial mobile elements, and other mechanisms, like hardening and strain aging [13]. As the LAS is subjected to a relatively high temperature, the amount of P on the grain boundaries increases with aging time. P segregation to grain boundaries is connected to an increase in the ratio of intergranular fracture and a larger shift in DBTT. A larger P content in the matrix enhances the P segregation to the grain boundaries, which is also dependent on the initial P content on the grain boundaries [7,13–16]. However, a larger P content in the matrix (0.007 versus 0.016 %) does not always lead to a larger shift in DBTT [14].

Besides the chemical composition and the aging temperature, thermal embrittlement is affected by the heat treatment, the resulting microstructure and aging time [5,9,17,18]. Typically, due to the heat treatment, the coarse-grained weld metal and heat-affected zone (HAZ) are considered to be more prone to thermal aging [13]. Compared to the base metal (BM), the sensitivity of the HAZ to thermal aging can be 3–6 times higher at 330 °C [19]. BMs are considered less vulnerable to temper embrittlement due to a finer prior austenitic grain size and the heat treatment consisting of quenching and tempering. Lower DBTTs are obtained when the grain size is smaller, 66 μm compared to 430 μm [14]. Yet, the shift in DBTT is not always dependent on the grain size. For the HAZ of a submerged-arc weld with 18MND5 as BM, the largest shift is reported to occur at 1 mm from the fusion boundary in the fine-grained region, and not in the grain-coarsening region [16].

Related to thermal aging of NG Alloy 52 DMWs, the DBTT shifts in HAZ of the LAS are difficult to assess. The HAZ consists of fine microstructural regions with varying mechanical properties, grain sizes and different tendencies for thermal embrittlement. In addition, the adjacency of the Ni-base weld metal can affect the sensitivity for thermal embrittlement. The previous investigations on

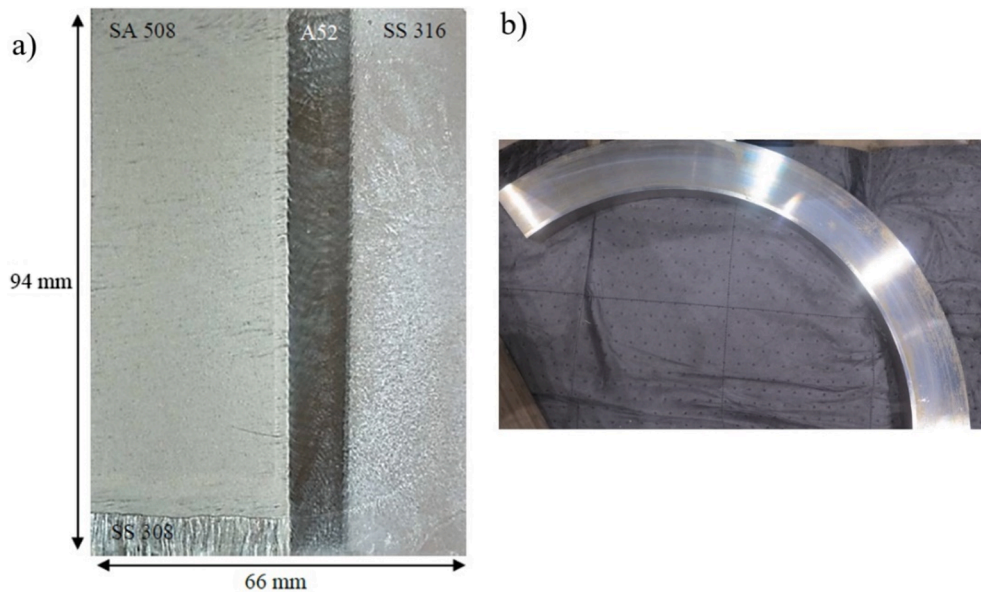


Fig. 1. NG Alloy 52 DMW. a) Cross-section of the weld. b) Section cut from the full-scale pipe mock-up.

Table 1

Chemistry of the materials.

Mock-up	C	Mn	Si	Ni	Cr	Mo	Cu	S	P	Al	V	Co	As	Sn
LAS, SA 508	0.18	1.44	0.19	0.77	0.11	0.49	0.060	0.001	0.005	0.02	< 0.01	0.01	0.003	0.003
WM, Alloy 52	0.002	0.26	0.15	59	30	<0.01	<0.01	0.0007	<0.005	0.66		<0.01	–	–

thermal embrittlement of the Alloy 52 DMWs mainly focus on characterization of the microstructural changes, and fracture mechanical changes at a distance of 0.3 mm from the fusion boundary close to the grain-refined region of the HAZ [20,21]. The fracture toughness in the near interface zones to the fusion boundary can be sensitive to the notch location and the fracture toughness behavior and shifts in DBTT closer to the fusion boundary need to be systematically studied and understood.

The shift in DBTT can be either determined using impact toughness or fracture toughness-based testing. An impact toughness test measures the energy consumed to initiate, propagate and arrest a crack. Typically, a T_0 fracture toughness test in the DBTT region describes the stress intensity required for initiation of brittle fracture. When the impact testing is done with an instrumented device, it gives the possibility to separate the initiation and arrest portions of the result. In previous investigations on DMWs, the arrest properties have not been investigated.

In this study, the focus is on characterization of thermal aging effects on the fracture properties next to the fusion boundary in the LAS, SA 508, of a NG Alloy 52 DMW. The DMW is subjected to accelerated aging at 400 °C for 5 000 h, 10 000 h and 15 000 h. The cracks and notches of the specimens are placed nominally 0.1 mm from the fusion boundary. Both fracture toughness testing according to ASTM E1921 and instrumented impact toughness testing (ISO 179 and ISO 148–1) are performed. The results show different shifts depending on the characterization methods. The mechanistic differences of the results are discussed.

2. Materials and methods

2.1. Material and component

An industrially manufactured 1:1 scale DMW safe-end pipe mock-up is investigated, Fig. 1. The thickness of the mock-up pipe is 94 mm. The inner diameter of the mock-up pipe is 920 mm and outer diameter is 968 mm. The width of the pipe is 66 mm. The mock-up consists of SA 508 LAS BM, Alloy 52 weld metal, AISI 316L stainless steel and AISI 308 cladding on top of the LAS part on the inner surface. Approximately 12 mm of the inner diameter was cut away to remove the cladding and HAZ of the cladding. Table 1 shows the chemical compositions of the base and weld materials. The fusion boundary between SA 508 and Alloy 52 is located roughly in the middle of the mock-up and is the focus of this study.

The weld was manufactured by applying NG gas tungsten arc welding (GTAW) and using Alloy 52 as welding consumable. The joint was welded one bead per layer without any buttering layer. After welding, the weld received a PWHT at 550 °C for 890 min and at 610 °C for 458 min.

The mock-up was thermally aged at 400 °C for 5 000 h, 10 000 h and 15 000 h. The temperature was monitored during thermal

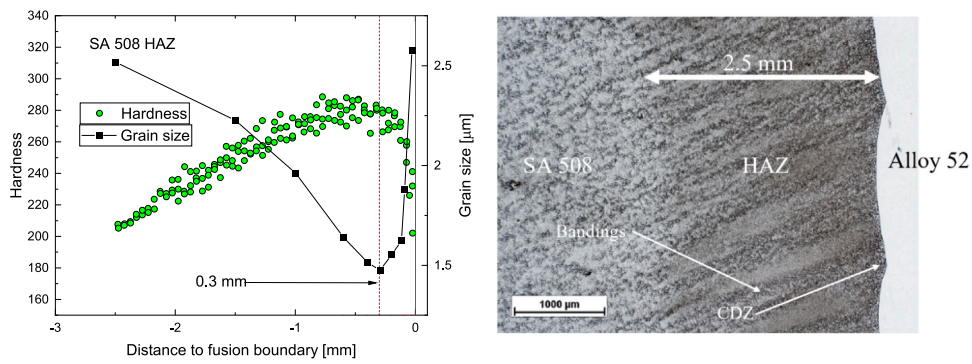


Fig. 2. The change in hardness and grain size in SA 508 HAZ adjacent to the fusion boundary. b) The macrostructure of the fusion boundary region [24].

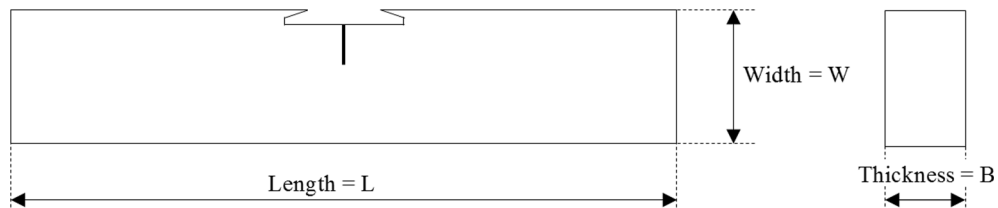


Fig. 3. T_0 characterisation is based on SE(B) specimens: 5 mm thick, 10 mm wide and 40 mm span.

Table 2

Test matrix for testing of fracture properties.

Test type	Fracture toughness	Impact toughness
Applied standard	ASTM E1921	EN ISO 148-1
Specimen type and dimensions	5x10 SE(B)	10x10 CVN
Orientation	T-L	T-L
Amount of specimens	10-15/condition	14-16/condition
Notch/crack location	LAS/weld metal fusion boundary, approximately 0-0.3 mm from the fusion boundary	
Investigated condition	Reference condition, thermally aged 5 000 h, 10 000 h and 15 000 h at 400 °C	

ageing using thermocouples, which stayed within about ± 1 °C during most of the thermal treatment. The ageing times and temperature were determined based on the assumption that P segregation is the main embrittlement mechanism. P segregation is enhanced at 400 °C without changing its degradation mechanism compared to the operation temperature of the DMW component at 325 °C [22]. According to Joly *et al.*, the ageing time of 10 000 h at 400 °C is representative to 60 years of operation, when P segregation is considered as the main degradation mechanisms [20].

Based on previous work for the DMW investigated in this study, Fig. 2 shows the variation in average hardness and grain size of the HAZ of the LAS. Thermal aging does not have a significant effect on hardness of the HAZ. The grain size reaches a minimum and hardness a maximum at 300 μm from the fusion boundary, the grain-refined region. Towards the base material from the maximum hardness location, the grain size and the hardness change gradually. In the fusion boundary region, <300 μm from the fusion boundary, the largest grains are located next to the fusion boundary, the grain-coarsening region. Fig. 2 shows the macrostructure of the HAZ and the BM consisting of segregation lines. The carbon-depleted zone (CDZ) next to the fusion boundary of this DMW is estimated to be 100 μm wide. [23].

For characterization of T_0 reference temperature for the DBTT region, 5×10 (thickness = 5 mm, width = 10 mm, length = 50 mm) single edge-notched bend (SE(B)) specimens were applied, Fig. 3. For characterization of impact toughness, standard size of 10×10 mm² (thickness = 10 mm, width = 10 mm, length = 55 mm) Charpy-V notch (CVN) specimens were used. The crack orientation for the SE(B) specimens and the CVN specimens is in the T-L direction (transverse - longitudinal), with the same direction as a through-wall crack. The SE(B) specimens were side grooved. The cracks of the SE(B) specimens and the notches of the CVN specimens are nominally located in the HAZ of the LAS, 100 μm from the fusion boundary. The cracks are parallel to the fusion boundary. Table 2 shows the test matrix.

The specimens were extracted from the mock-up by first cutting the mock-up in thinner slices with an electro-discharge wire cutter (EDWC). The location of the notch of the specimens relative to the fusion boundary was marked on the slice through a magnifying glass. The weld was etched with 3 % nital to reveal the fusion boundary. The marked location was the starting point for the EDWC.

2.2. Fracture toughness-based reference temperature, T_0

The fracture toughness testing was performed in the DBTT region according to ASTM E1921 “Standard Test Method for Determination of Reference Temperature, T_0 , for Ferritic Steels in the Transition Range”. [24,25] Before testing, the specimens were pre-cracked by fatigue to the initial crack length over specimen width ratio a_0/W of 0.5, using a RUMUL resonant testing machine. The maximum value of applied stress intensity factor, K_{max} , was kept below $15 \text{ MPa}\sqrt{\text{m}}$ during fatigue pre-cracking. The fracture toughness testing was performed using a MTS universal servo-hydraulic testing machine equipped with a 10 kN load cell. The maximum force varied between 1.7 and 2.9 kN. The crack mouth opening displacement (CMOD) was measured using Epsilon 3541-003 M-040 M-LHT clip gauge, with a measurement range of $-1/+4 \text{ mm}$. The loading rate was kept in the quasi-static range, $0.3\text{--}1 \text{ MPa}\sqrt{\text{m/s}}$.

After testing, the specimens were soaked in liquid nitrogen and broken into two halves to measure the crack lengths corresponding to the load instability moment. There is no prior ductile crack growth before initiation of brittle fracture. The crack length and crack front straightness were checked before calculation of T_0 .

The quality of the results was assessed after testing. All the T_0 specimens fractured by the brittle fracture mechanism and the brittle fracture initiated without significant ductile crack growth. The force–displacement curves are continuous and temperature control quality was acceptable. The cracks of the specimens were located in the HAZ. For some specimens, the crack front straightness criterion was not fulfilled, and these results are discarded, see Section 4.1. The T_0 was determined using the multi-temperature procedure as described in ASTM E1921, where the results exceeding the maximum K_{Jc} capacity, $K_{Jc,limit}$ were censored. The limit is there to maintain a condition of high crack-front constraint at fracture.

2.3. Impact toughness

The testing was performed according to EN ISO 148-1 using an instrumented impact pendulum, PSW300, with the nominal impact energy of 300 J and the impact velocity of 5.4 m/s [26]. The pendulum was equipped with a digital angle encoder having the angle counting resolution of 160 000 pulses/360°. An ISO/DIN geometry impact striker (2 mm striker) was used in the pendulum.

The specimens were heated and cooled in a well-agitated liquid bath. Depending on the test temperature, either petrol ether ($T < -80^\circ\text{C}$), ethanol ($-80^\circ\text{C} < T < +70^\circ\text{C}$) or silicon oil ($T > +70^\circ\text{C}$) as the heating or cooling medium was used. The bath temperature was measured with a calibrated thermocouple adjusted with a PDI-controller. The bath was heated electrically and cooled by circulating liquid nitrogen through a coil installed in the bath. The bath temperature was continuously monitored and recorded during the cooling and heating phases. The specimens were held at least 5 min at a stable temperature before testing. The temperature was measured with Fluke 52 II thermometer and a K-type SAB thermocouple.

The specimens were moved from the tempering bath into the pendulum anvil with a pneumatic equipment. The proper location of the impact after each test was checked from the specimen halves by setting the V-groove surfaces side by side and by checking the equality of the anvil marks on specimen front surface.

The instrumented impact test gives in addition to the impact energy the force–time signal. From the signal, the crack arrest force F_a was determined [27]. The arrest force F_a was applied to assess the crack arrest reference temperature, T_{Kla} , by using the correlation described in [28].

2.4. Metallography, crack path and fractography

The fracture surfaces of the tested T_0 and CVN specimens were optically imaged. Scanning electron microscopy (SEM) was used to determine the brittle fracture initiation sites of the T_0 specimens, and the fracture appearance of the impact toughness and fracture toughness specimens. The locations of the notches of the CVN specimens were optically determined from the side surfaces, and the crack locations of the T_0 specimens were determined using an optical profilometer, Sensofar PL μ 2300, relying on a non-contact, dual-technology sensor. The profile was used to determine the vertical distance between the initiation site and the fatigue pre-crack tip. The same crack location characterization procedure was applied as in [29].

For confirmation of the crack and notch locations, and to investigate the crack path behavior, some specimens were cut along the mid-plane. These cross-section samples were grinded using SiC papers up to 2 000 grit, polished using diamond polishing paste up to $0.25 \mu\text{m}$, and finally polished in a vibratory polisher using colloidal silica suspension. The surface was etched with 3 % nital to reveal the interface between the LAS and the Alloy 52 weld metal. The cross-sections were imaged using optical microscope and SEM.

3. Results

3.1. Fractography and crack location

First the fractography and crack location investigations are presented to get a general understanding of the fracture behavior for the investigated material. The crack path behavior affects the fracture toughness and the impact toughness.

3.1.1. T_0 Crack locations, path and initiation site

For most of the T_0 specimens, the fatigue pre-cracks are in the HAZ of the LAS. In few cases, the cracks are partially in the weld metal. Consequently, the fatigue pre-crack front is skewed and does not fulfil the crack front straightness requirement in few specimens. For most specimens, even if the cracks are farther from the fusion boundary in the HAZ, crack initiation occurs next to the fusion

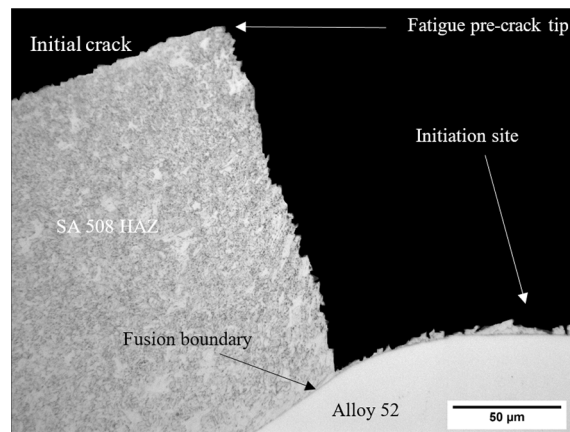


Fig. 4. In most instances, brittle fracture initiation occurs in the CDZ next to the fusion boundary, even if the fatigue pre-crack is farther away from the fusion boundary. The distance between the fatigue pre-crack tip and the fusion boundary is 159 μm .

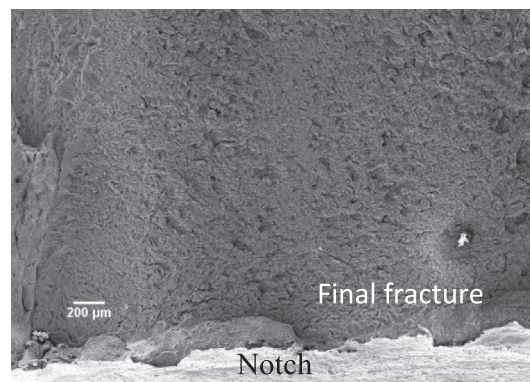


Fig. 5. A SEM image of a typical fracture surface showing the wavy fracture surface appearance following the weld fusion boundary. Specimen: CVN specimen, tested in reference condition, $E = 38 \text{ J}$, and $T = -30 \text{ }^\circ\text{C}$.

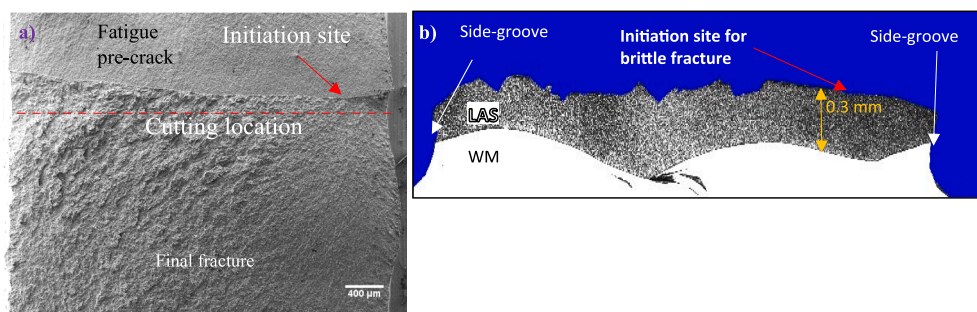


Fig. 6. Specimen with lower fracture toughness. Crack propagation 0.3 mm from the fusion boundary in the LAS. Specimen: test temperature is $-140 \text{ }^\circ\text{C}$, $K_{Jc(25 \text{ mm})}$ is $23 \text{ MPa}\sqrt{\text{m}}$ and material condition is aged for 15 000 h at $400 \text{ }^\circ\text{C}$. The cutting location of the cross-section sample, 6b, is marked with a red line in Fig. 6a.

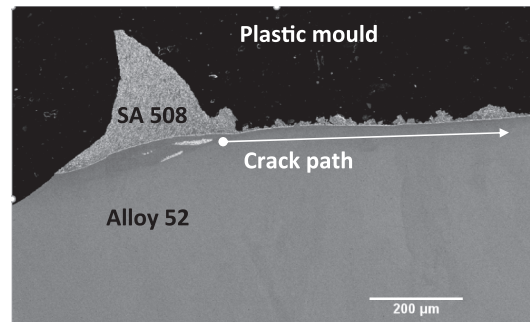
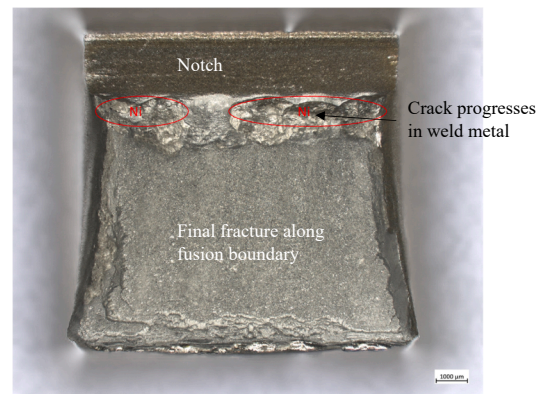
boundary, in the CDZ, 2–20 μm from the fusion boundary, and the final fracture occurs along the fusion boundary. Fig. 4 shows an example of a crack deviating to the fusion boundary and progressing along the fusion boundary. Also, the wavy features of the underlying bead structure are visible on the fracture surface (Fig. 5).

However, in four instances for the 15 000 h aged material, the brittle fracture initiation and crack progression occur in the HAZ 0.3 mm from the fusion boundary (see Fig. 6). On the fracture surface of those specimens, the wavy features of the fusion boundary are not observable, and the fracture surface is smooth without crack path deviation. For the different conditions, Table 3 summarizes the average distance of the fatigue pre-crack tip from the fusion boundary.

Table 3

Summary of the average crack locations relative to the fusion boundary and the transition temperatures for the different conditions.

Condition	Fatigue pre-crack location [mm]	T_0 based on ASTM E1921	T_0 corrected for crack location
Reference	0.05	-118	-118
5 000 h aged at 400 °C	0.07	-112	-105
10 000 h aged at 400 °C	0.12	-129	-111
15 000 h aged at 400 °C	0.2	-134	-109

**Fig. 7.** The cross-section for crack path assessment of a brittle CVN specimen. Specimen: reference condition, $E = 38$ J, $T = -30$ °C.**Fig. 8.** Partial crack growth in the weld metal of a CVN specimen before final brittle fracture along the fusion boundary. Specimen: testing temperature is 19 °C, impact energy is 109 J, and material condition is aged for 15 000 h at 400 °C.

3.1.2. Fracture path in CVN specimens

For the CVN specimens fractured in the transition region, the fracture surface shows a wavy appearance following the shape of the fusion boundary, as illustrated in Fig. 5. Fig. 7 shows that the brittle fracture initiates and propagates in LAS close, about 0–50 μm , to the fusion boundary, even if the notch is initially farther from the fusion boundary. The crack path behavior is similar to the fracture toughness specimens.

The scatter in the impact toughness results, presented in Section 4.3, is relatively high. The notches were visually confirmed to be located at or close to the fusion boundary. For some specimens due to notch location variations, the crack progresses slightly on the weld metal side before deviating to the fusion boundary. The resulting fracture surfaces have small weld metal ligaments close to the notch root, see Fig. 8. The crack path of specimens with higher impact energy grows first in the weld metal before brittle fracture initiation occurs on the LAS side.

3.2. T_0 Fracture toughness

Fig. 9 shows the T_0 results for the different conditions when the brittle crack initiates and progresses along the fusion boundary. In all the analyzed cases, the specimens fracture by the brittle fracture mechanism. The T_0 is -118 °C in reference condition, -111 °C for the 5 000 h, -129 °C for the 10 000 h and -134 °C for the 15 000 h aged material. Figs. 9 and 10 show the fracture toughness results for each condition separately and together, respectively. The fatigue pre-cracks for the 10 000 h and 15 000 h aged specimens are located farther from the fusion boundary compared to the reference and 5 000 h aged condition, see Table 3. Fig. 11 shows that the fracture

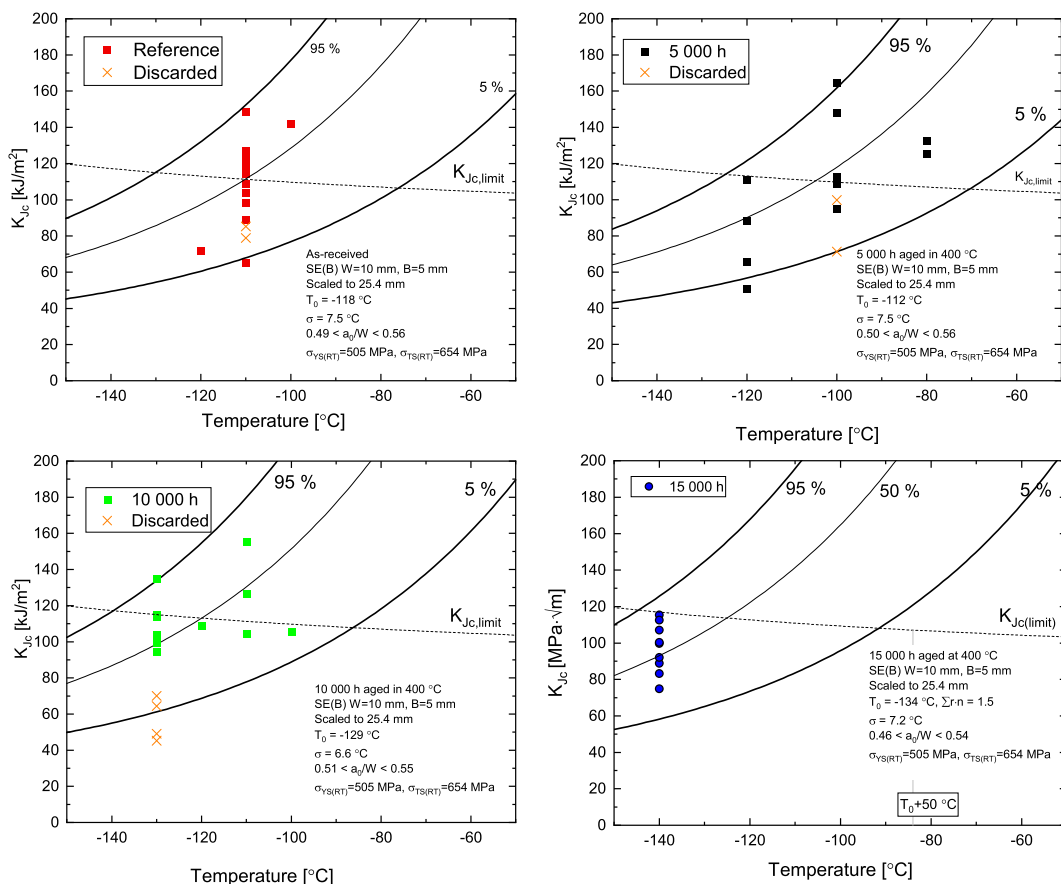


Fig. 9. T_0 analyses for reference, 5 000 h, 10 000 h and 15 000 h aged conditions. Some data points are discarded due to failure of the crack front straightness criteria. The values above the limit were censored when calculating T_0 .

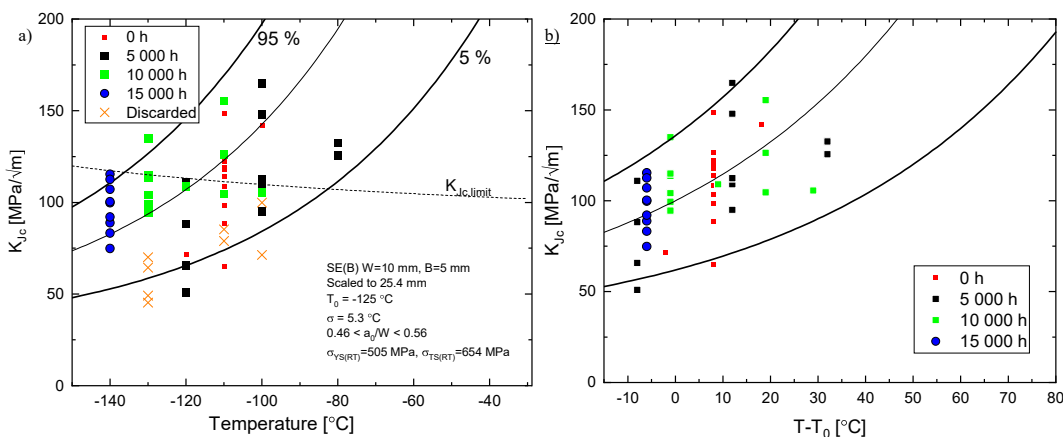


Fig. 10. a) all T_0 results with the crack path deviating towards the fusion boundary. b) the results normalized by T_0 . The censored results above $K_{Jc,limit}$ can be seen in Fig. 9.

toughness is higher when the crack-tip is farther from the fusion boundary and thus, the results are not directly comparable. Based on the method presented in [29], we corrected the results for 5 000 h, 10 000 h and 15 000 h thermally aged condition to estimate what the T_0 is if the pre-cracks are located 0.05 mm from fusion boundary, so that all results are comparable. Table 3 shows the values after applying the correction.

In contrary, for four specimens aged for 15 000 h, the crack initiation and propagation occur only in the HAZ approximately 0.3 mm

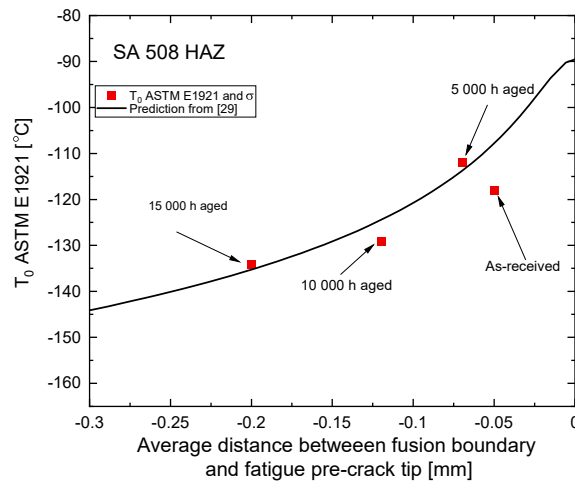


Fig. 11. T_0 as a function of the distance between fatigue pre-crack tip and fusion boundary.

Table 4

Specimens aged for 15 000 h with crack initiation and propagation in the HAZ, 0.3 mm from the fusion boundary.

Temperature [°C]	Fracture toughness, $K_{Jc(25.4 \text{ mm})}$ [MPa $\sqrt{\text{m}}$]
-140	43
-140	40
-140	24
-140	38

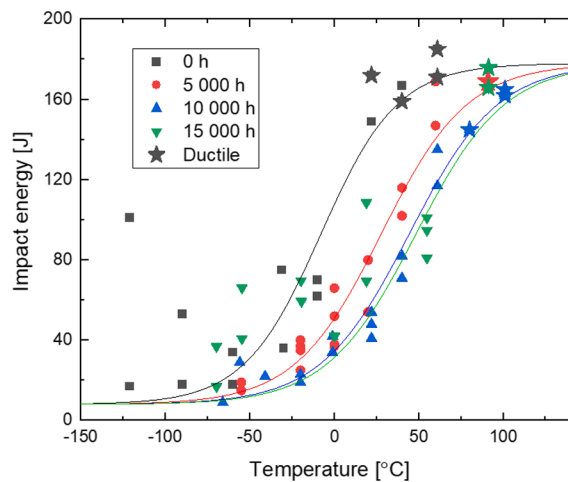


Fig. 12. Transition curves of impact energies for reference, 5 000 h, 10 000 h and 15 000 h aged conditions. The star symbols indicate 100 % ductile fracture.

from the fusion boundary (see Fig. 6). The fracture toughness is lower compared to the specimens with crack path deviation to the fusion boundary. The average fracture toughness is 36 MPa $\sqrt{\text{m}}$ at -140°C , (see Table 4). A valid T_0 estimate according to ASTM E1921 cannot be determined with only 4 observations. Since the crack path behavior differs from the other specimens, the results are treated separately. Evidently, the results show that as the distance to the fusion boundary increases a point is reached where the properties of the hard zone dominates the fracture behavior and the crack does not deviate to the fusion boundary.

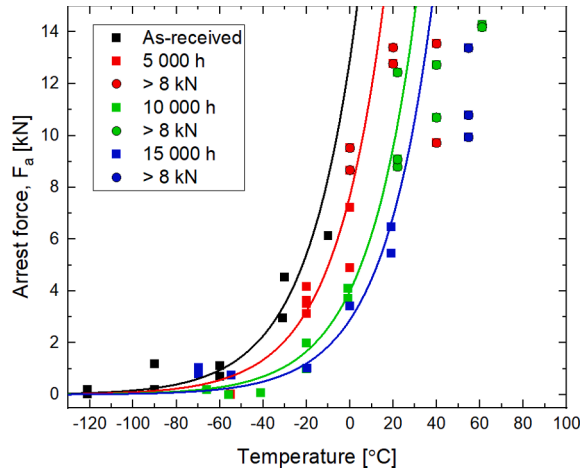
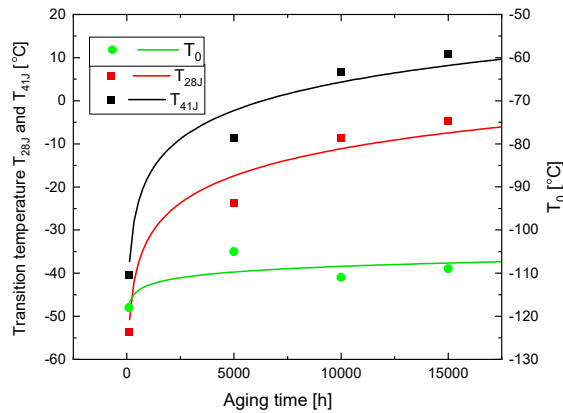
3.3. Impact toughness

Fig. 12 shows the impact energy-based transition curves for reference, 5 000 h, 10 000 h and 15 000 h aged conditions. The

Table 5

Summary of transition temperatures and upper shelf values measured for the reference, 5000 h, 10000 h and 15 000 h aged conditions.

Material	T _{28J}	T _{41J}	USE	T _{Fa4kN}	T _{KIa}
	(°C)	(°C)	(J)	(°C)	(°C)
Reference	-54	-40	172	-27	-16
Ageing, 5 000 h	-24	-9	168	-15	-4
Ageing, 10 000 h	-9	7	164	0	11
Ageing, 15 000 h	-5	11	171	7.5	19

**Fig. 13.** F_a - T curves for the different conditions.**Fig. 14.** Effect of aging time at 400 °C on transition temperature.

transition curve shifts to the right as the material aging time increases. The scatter is relatively high for the reference and 15 000 h aged conditions, due to variations in notch location and partial crack growth in the weld metal, as explained in Section 4.1.2. Due to this reason, for the 15 000 h aged condition, the location of the transition curve for the HAZ cracks was estimated based on the lower boundary results. Table 5 summarizes the T_{42J} and T_{28J} transition temperatures and upper-shelf energy (USE). In the transition curve fitting process, the USE was determined by calculating an average USE for the different conditions, since previous results indicate that thermal aging does not affect significantly the USE [23].

Fig. 13 shows that the arrest force values decrease and that the arrest transition curve shifts towards the right with increasing aging time. A power law equation, the transition curve, was fitted to the arrest force, F_a , data

$$F_a = 4 * \exp\left(\frac{T - T_{Fa4}}{A}\right) \quad (1)$$

where T_{Fa4kN} is the arrest force at the temperature corresponding to 4 kN connected to a crack jump halfway through the component, T

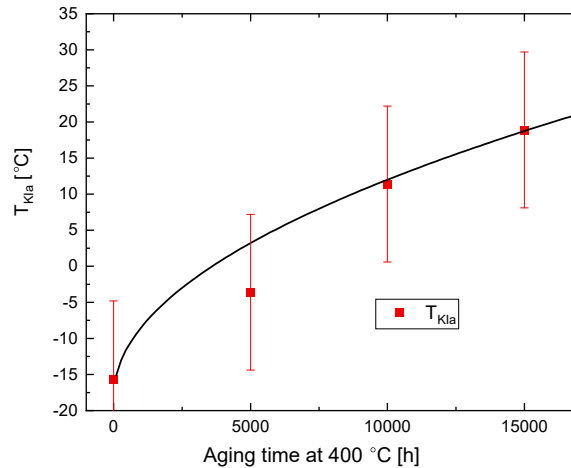


Fig. 15. Shift in arrest reference temperature T_{Kla} . A common uncertainty, $2\sigma = 10.8$ °C, for the different conditions was calculated based on the upper part of the transition curve. The transition curves are presented in Fig. 13.

is the test temperature and A is a fitting parameter. The fitting parameter was selected to be the same for all conditions, $A = 23$. The results exceeding 8 kN were not included to the fitting since at high crack arrest forces, where the crack jump is small, the results may be affected by the initiation force. Also specimens with significant crack growth were excluded by applying F_u/F_m (initiation force/maximum force) > 0.7 criteria, otherwise the measured crack arrest force can be lower than the true crack arrest force. [30].

4. Discussion

4.1. Shifts in fracture toughness and impact toughness

Fig. 14 shows the difference in the shifts for crack location corrected T_0 and impact toughness based T_{28J} and T_{41J} . The shift after thermal aging at 400 °C for 15 000 h is ~ 50 °C based on impact toughness testing and 10 °C based on fracture toughness testing. The effect of aging on the shift in impact toughness appears to slow down after 10 000 h of thermal aging. The T_0 shift is of the same order as the standard deviation of the T_0 estimate, but the crack location corrected T_0 values for the aged conditions are systematically above the reference condition. The effect of thermal aging on T_0 is marginal.

The different shifts from the impact toughness and fracture toughness testing can be explained by the nature of the test methods. The fracture toughness describes the stress intensity required to initiate brittle fracture in the DBTT region, whereas the impact toughness describes the energy required to initiate, propagate and arrest a crack. Additionally, the fracture toughness specimens are more sensitive for crack/notch location relative to the fusion boundary in the HAZ compared to impact toughness specimens since the fracture process zone of an impact toughness specimen with a blunt V-notch samples a larger region. [30] However, the results show that if part of the notch of an impact toughness specimen is in the weld metal, the impact toughness increases significantly. In addition, the applied crack location correction procedure reduces this difference.

Impact toughness and fracture toughness can be affected differently by the aging mechanism. The assumed main thermal aging mechanism is P segregation observed to be the main embrittlement mechanism for a similar Alloy 52 DMW [20]. Due to thermal aging, the P content increases on the grain boundaries leading to a shift in transition temperature and sometimes to an increase in intergranular fracture [4,16]. Previously, for the same DMW [23], we have observed that the fraction of intergranular fracture increases on the fracture surface as a function of aging time. Noticeably, brittle fracture initiation for the investigated material is defined by a primary initiation site indicating preservation of the weakest link assumption. P segregation to grain boundaries can mechanically affect more the crack propagation and arrest properties than crack initiation.

The impact toughness testing was done with an instrumented impact hammer enabling characterization of the effect of aging on the crack arrest reference temperature, T_{Kla} , estimated based on

$$T_{Kla} = T_{Fa4kN} + 11.4 \text{ [}^\circ\text{C]} \pm \sigma = 12.0^\circ\text{C} \quad (2)$$

Fig. 15 shows that the crack arrest reference temperature increases with 35 °C after aging at 400 °C for 15 000 h, which is 15–16 °C smaller than the shift in T_{28J} or T_{41J} . Based on the results, thermal ageing appears to affect more the crack arrest properties of the fusion boundary region than the brittle fracture initiation properties. A similar result is observed in [31] where a reactor pressure vessel LAS of a hydrotreating reactor in an oil refinery operated at 400 °C for 17 years shows a 60–70 °C shift in impact toughness, whereas the T_0 remains practically unchanged.

Structural integrity codes (API, ASME, BS 7910, R6, SINTAP/FITNET) allow the DBT toughness assessment to be done directly or indirectly using T_0 , or an impact toughness-based transition temperature estimate. The results from this study underline the mechanistic differences in these two methods yielding different DBTT shifts due to aging. The T_0 reference temperature describes more

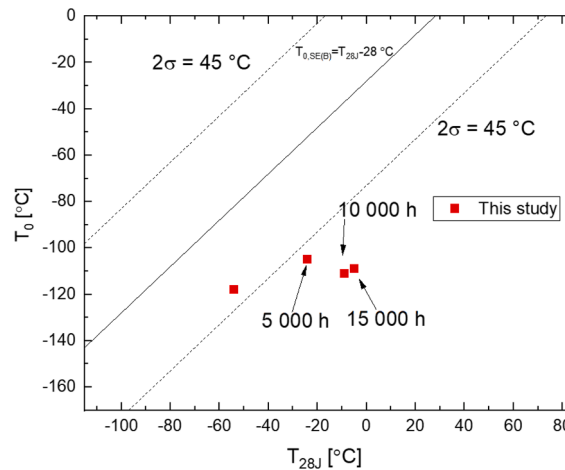


Fig. 16. Correlation between impact toughness based T_{28J} and fracture toughness based T_0 .

Table 6

Comparison of two similar DMWs.

	DMW from this study	DMW from [20] and [21]
Shift in T_0 [°C]	10	27
T_0 in non-aged condition [°C]	-118	-153
Average distance of the crack to the fusion boundary	≈ 0.1 mm	≈ 0.3 mm
Crack propagation	Deviates to the fusion boundary and grows along the fusion boundary	No evident jumps
Chemistry	Ni = 0.71, Mn 1.44 %, P = 0.005 %	Ni = 0.71, Mn 1.46 %, P = 0.007 %
PWHT	14.8 h at 550 °C and 7.7 h at 610 °C	6 + 10 h at 600 °C
Size of the CDZ	100 μ m	150 μ m
Microstructural location of the crack	In average, the cracks are in the CDZ	Less than 150 μ m in average from the CDZ
Specimen	5x10 SE(B)	1 T C(T)

precisely the brittle fracture initiation process, and the resulting Master Curve is directly applicable without the need for conversion. For the investigated material, the impact toughness-based transition temperature gives a more conservative estimate of the DBTT. In this case, impact toughness testing can be applied to get a first estimate of the DBTT, if better precision is needed fracture toughness testing is recommended.

4.2. T_0 And T_{28J} dependence

In [32], Kocak *et al.* give a generic dependence for T_0 and T_{28J} , $T_0 = T_{28J} - 18$ °C, with a standard deviation of 15 °C. The assessment in [30] shows that the dependence is applicable for C(T) specimens, but the standard deviation is 22.5 °C. And the same correlation for SE(B) specimens is an offset of 10 °C due to the constraint effect.

Fig. 16 shows that the T_0 and T_{28J} values obtained from this study are closer to the lower part of the 2σ scatter band in the reference condition. The difference to the general dependence grows as the material ages since aging affects more T_{28J} than T_0 . The $T_0 = T_{28J} - 28$ °C dependence gives a conservative estimate of the T_0 values. The cause for the difference could be in future investigated through comparative material simulations of impact and fracture toughness specimens with the crack/notch at a soft/hard interface. The aim would be to compare how the softer weld metal affects the stress fields ahead of the crack and notch, and under different loading rates.

4.3. Comparing the DBTT shifts to similar materials

In this study, the shift in T_0 is marginal. In [20] and [21], they investigated a similar Alloy 52 DMW. The material was aged for 10 000 h at 400 °C and for 50 000 h at 350 °C. The shift in T_0 is higher compared to this study, ΔT_0 is approximately 30 °C in both cases, and the absolute T_0 values are lower, see Table 6. From chemical perspective the materials are similar. The P content differs slightly, but not significantly according to previous investigations [4].

One possible reason for the difference in fracture toughness behavior is the PWHT. The PWHTs differ between the two DMWs. The PWHT of mock-up investigated in [20] and [21] lasted 6 + 10 h at 600 °C, compared to 14.8 h in 550 °C and 7.7 h at 610 °C for the DMW from this study. Consequently, the CDZ is reported to be 50 μ m wider in [20] and [21]. The PWHT in [20] and [21] was

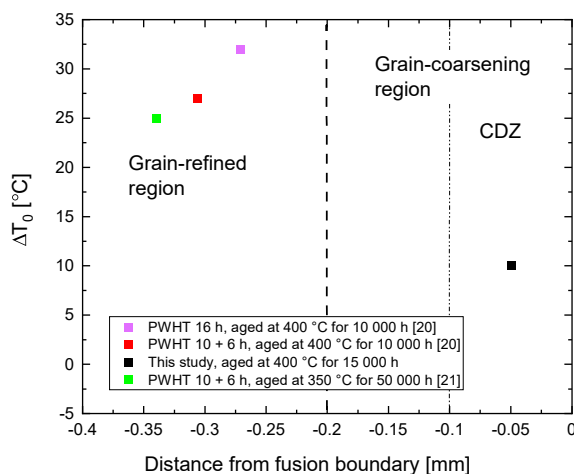


Fig. 17. Shifts in ΔT_0 as function of distance to fusion boundary for two different Alloy 52 DMWs. [2021].

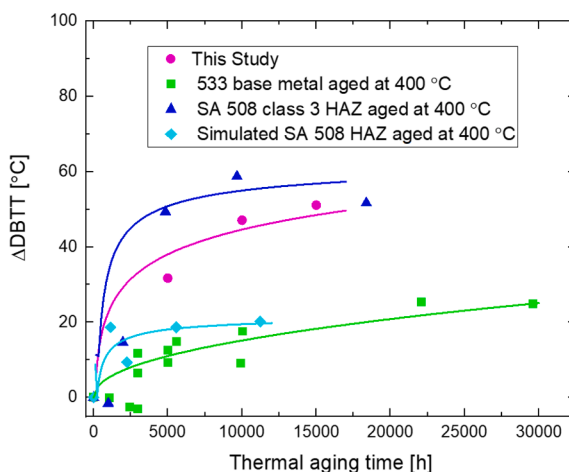


Fig. 18. DBTT shifts for 533 BM, SA508 HAZ of a similar metal weld and HAZ of the DMW from this study.

optimized to enhance the effect of thermal ageing on the reference temperature shift.

The shift in T_0 can also be affected by crack location. Compared to this study, the average crack location is in [20] and [21] farther from the fusion boundary closer to the grain-refined region, see Fig. 17. In another study [16], Joly *et al.* reported a larger shift in DBTT for the grain-refined region than the grain-coarsening region of 18MND5 HAZ (similar to SA 533). Noticeably, for the investigated DMW after 15 000 h of aging, a lower fracture toughness is measured 0.3 mm from the fusion boundary when the crack no longer deviates to the fusion boundary, as explained in Sections 4.1.1 and 4.2. Yet, the observation cannot be connected to thermal aging, since there is no reference data for that region.

For the investigated material, as long as the crack deviates to the fusion boundary, the fracture toughness increases with the distance of the crack-tip to the fusion boundary. Though in [20] and [21], they do not report similar crack path deviations towards the fusion boundary and fracture toughness does not have a similar dependence on crack location. Brittle fracture initiation appears to occur randomly in the HAZ. Future investigations could focus on better understanding the fracture path and aging behavior farther from the fusion boundary, and the specimen size effects. In this study, the fracture toughness was measured with smaller specimens, see Table 6. Specimens of varying size have proportional differences in process zone size, and thus, are affected in a different way by the surrounding regions such as the softer weld metal and not necessary as affected by the local microstructural regions.

Fig. 18 compares impact toughness-based transition temperature shifts due to thermal aging at 400 °C for the Alloy 52 DMW from this study, a 533 BM [16,18], a grain-coarsened HAZ of SA 508 class 3 RPV weldment, [19], and a simulated grain-coarsened HAZ of SA 508 [18]. The 533 BM is similar to the SA 508 LAS. Compared to the BM, the shifts for the DMW are >30 °C higher after 10 000 h aging. The grain size and the P content is smaller in the CDZ of the DMW than for the 533 BM, see Table 7. A significant difference between the BM and the DMW is the PWHT and the heating during welding.

The transition temperature shift for the DMW is similar to the grain-coarsened HAZ of SA 508. In both instances, the shift saturates. The notches of the DMW are also located in the grain-coarsened HAZ. Table 7 summarizes key parameters for the materials affecting

Table 7

Key parameters affecting thermal aging. The effect of welding parameters and PWHT on thermal embrittlement could not be analyzed.

	CDZ of the DMW	533 BM	GC HAZ of a WM	Simulated CG HAZ
Material	BM is SA 508	SA 533	SA 508	SA 508
P %	0.002 for BM and 0.005 for WM	0.005–0.012	0.006 for BM and 0.019 for WM	0.007
Ni %	0.77 for BM and 59 for WM	0.6–0.7	0.8	0.75
Grain size [um]	2.5 close to the fusion boundary	4–22 μm	22, typical for RPVs	125

the sensitivity to thermal aging. The bulk P content is slightly smaller for the DMW, and the grain size also, typically decreasing the sensitivity to thermal aging but not making a significant difference in this case.

5. Conclusions

In this study, we investigated an Alloy 52 dissimilar metal weld (DMW). The DMW consists of SA 508 low-alloy steel (LAS) base metal, Alloy 52 weld metal, AISI 316L stainless steel. The fracture properties were characterized according to ASTM E1921 to obtain reference temperature T_0 and EN ISO 148–1 to obtain T_{28J} and T_{41J} . The impact toughness testing was done using an instrumented impact hammer to obtain the arrest force and arrest toughness. The material was aged at 400 °C for 5 000 h, 10 000 h and 15 000 h. The crack was nominally placed at the fusion boundary between the weld metal and the LAS.

- The initiation of brittle fracture tends to occur next to the fusion boundary in the carbon-depleted zone. For cracks farther from the fusion boundary, in the HAZ, the crack deviates to the fusion boundary and progresses in that region, in most cases.
- T_0 results in a lower shift than impact toughness. The crack location corrected T_0 shift is 10 °C after 15 000 h at 400 °C, whereas ΔT_{28J} is 49 °C. The ΔT_{28J} and ΔT_{41J} saturate after 10 000 h at 400 °C, while ΔT_0 appears to saturate after 5 000 h.
- The thermal aging mechanism can affect more the crack arrest and propagation mechanism than the initiation mechanism. The crack arrest toughness reference temperature increases with 35 °C after 15 000 h at 400 °C.

CRedit authorship contribution statement

Sebastian Lindqvist: Writing – original draft, Methodology, Formal analysis, Conceptualization. **Zaiqing Que:** Writing – review & editing. **Pekka Nevasmaa:** Writing – review & editing. **Noora Hytönen:** Writing – review & editing, Methodology.

Declaration of Competing Interest

The authors declare the following financial interests/personal relationships which may be considered as potential competing interests: [The project was funded and supported from the Finnish (Teollisuuden Voima Oyj), Swedish (Ringhals AB and OKG AB) partners and VTT Technical Research Centre of Finland. Finnish and Swedish regulatory bodies participated to the final project meeting.].

Data availability

Data will be made available on request.

Acknowledgments

The authors wish to express their gratitude for the funding and support from the Finnish (Teollisuuden Voima Oyj), Swedish (Ringhals AB and OKG AB) partners and VTT Technical Research Centre of Finland within the FEMMA research project. Thank you also to Jorma Hietikko, Laura Sirkiä and Jari Lydman.

References

- [1] MacDonald DD, Cragnolino GA. Corrosion of steam cycle materials. In: Cohen P, editor. ASME Handb. water Technol. Therm. power Syst., ASME: New York, Ny, USA; 1989, p. 659–2031.
- [2] Aaltonen P, Hänninen H. Water chemistry and behavior of materials in PWRs and BWRs. IAEA-TECDOC-965, Vienna, Austria: IAEA; 1997, p. 205–22.
- [3] Ehrstén U. Corrosion and stress corrosion cracking of austenitic stainless steels. In: Allen TR, Stoller RE, Yamanaka S, editors. Compr. Nucl. Mater., Amsterdam, The Netherlands: Elsevier Ltd; 2012, p. 93–104.
- [4] IAEA. Integrity of Reactor Pressure Vessels in Nuclear Power Plants: Assessment of irradiation embrittlement effects in reactor pressure vessel steels. 2009.
- [5] Server WL, Brumovský M. International Review of Nuclear Reactor Pressure Vessel Surveillance Programs. STP1603 2018. <https://doi.org/10.1520/stp1603-eb>.
- [6] Williams T, Nanstad R. Structural alloys for nuclear energy applications. Low-alloy steels 10. Elsevier; 2019. Doi: 10.1016/B978-0-12-397046-6.00010-1.
- [7] Nikolaeva AV, Nikolaev YA, Kryukov AM. Grain boundary embrittlement due to reactor pressure vessel annealing. J Nucl Mater 1994;211:236–43. [https://doi.org/10.1016/0022-3115\(94\)90352-2](https://doi.org/10.1016/0022-3115(94)90352-2).
- [8] Gurovich BA, Chernobaeva AA, Erak DY, Kuleshova EA, Zhurko DA, Papina VB, et al. Chemical composition effect on VVER-1000 RPV weld metal thermal aging. J Nucl Mater 2015;465:540–9. <https://doi.org/10.1016/j.jnucmat.2015.06.010>.
- [9] Corwin W, Nanstad RK, Alexander D, Odette GR, Stoller RE, Wang JA. Thermal embrittlement of reactor vessel steels n.d.

- [10] Shtrombakh YI, Gurovich BA, Kuleshova EA, Frolov AS, Fedotova SV, Zhurko DA, et al. Effect of Ni content on thermal and radiation resistance of VVER RPV steel. *J Nucl Mater* 2015;461:292–300. <https://doi.org/10.1016/j.jnucmat.2015.02.023>.
- [11] Erak DY, Zhurko DA, Papina VB. Interpretation of accelerated irradiation results for materials of WWER-1000 reactor pressure vessels 2013;45:424–32.
- [12] Boåsen M, Lindgren K, Öberg M, Thuvander M, Faleskog J, Efsing P. Analysis of thermal embrittlement of a low alloy steel weldment using fracture toughness and microstructural investigations. *Eng Fract Mech* 2022;:108248. <https://doi.org/10.1016/j.engfracmech.2022.108248>.
- [13] Vatter IA, Hipsley CA, Druce SG. Review of thermal ageing data and its application to operating reactor pressure vessels. *Int J Press Vessel Pip* 1993;54:31–48. [https://doi.org/10.1016/0308-0161\(93\)90126-E](https://doi.org/10.1016/0308-0161(93)90126-E).
- [14] Nanstad RK, McCabe DE, Sokolov MA, English CA, Ortner SR. Investigation of temper embrittlement in reactor pressure vessel steels following thermal aging, irradiation and thermal annealing. *Eff Radiat Mater* 20h Int Symp ASTM STP 1405 2001.
- [15] Nakata H, Fujii K, Fukuya K, Kasada R, Kimura A. Grain boundary phosphorus segregation in thermally aged low alloy steels. *J Nucl Sci Technol* 2006;43:785–93. <https://doi.org/10.1080/18811248.2006.9711160>.
- [16] Joly P, Roch F, Primault C. Effect of thermal ageing on properties of pressure vessel low alloy steel. PVP2013-97643. *Am Soc Mech Eng Press Vessel Pip Div PVP* 2013;7:1–8. Doi: 10.1115/PVP2013-97643.
- [17] Hudson JA, Druce SG, Gage G, Wall M. Thermal ageing effects in structural steels. *Theor Appl Fract Mech* 1988;10:123–33.
- [18] Druce SG, Gage G, Jordan G. Effect of ageing on properties of pressure vessel steels. *Acta Metall* 1986;34:641–52. [https://doi.org/10.1016/0001-6160\(86\)90179-3](https://doi.org/10.1016/0001-6160(86)90179-3).
- [19] Gage G, Druce SG, Popkiss EW. Thermal ageing embrittlement of the heat-affected zone in a PWR RPV steel weldment. Proceedings of the topical meeting on nuclear power plant life extension 1988.
- [20] Joly P, Yescas M, Keim E. Fracture toughness in the ductile-brittle transition and thermal ageing behavior of decarburized heat affected zone of alloy 52 dissimilar metal welds of nuclear components. PVP2014-29044. *Proc ASME-2014 Press Vessel Pip Conf* 2014;PVP2014:1–13.
- [21] Yescas M, Joly P, Roch F. Thermal aging assessment and microstructural investigations of Alloy 52 dissimilar metal welds for nuclear components. PVP2019-93120. *Proc ASME 2019 Press Vessel Pip Conf* 2019;PVP2019:1–9.
- [22] Leverenz R, Gerhard L, Göbel A. The European Pressurized Water Reactor : A Safe and Competitive Solution for Future Energy Needs. *Proc Int Conf Nucl Energy New Eur Portorož, Slov Sept* 6-9, 2004 2004;1:1–7.
- [23] Ahonen M, Lindqvist S, Sarikka T, Mouginot R, Leskelä E, Lydman J, et al. Thermal ageing and mechanical performance of narrow-gap dissimilar metal welds, VTT technology report 333. Espoo: 2018. <https://www.vtt.fi/inf/pdf/technology/2018/T333.pdf>.
- [24] ASTM E1921-15. Standard test method for determination of reference temperature, T₀, for ferritic steels in the transition range. ASTM E1921-15. ASTM International; 2015.
- [25] ASTM E1921-20. Standard Test Method for Determination of Reference Temperature, T₀, for Ferritic Steels in the Transition Range. ASTM Int 2020.
- [26] ISO 148. ISO 148-1. Metallic materials - Charpy pendulum impact test - Part 1 test method. 2016.
- [27] ISO 179-2. ISO 179-2:2020(en) Plastics - determination of Charpy impact properties - Part 2: instrumented impact test. 2020.
- [28] Wallin K. Descriptive potential of Charpy-V fracture arrest parameter with respect to crack arrest KIa. vol. 221. 1993.
- [29] Lindqvist S, Ahonen M, Lydman J, Arffman P, Hänninen H. A crack-location correction for T₀ analysis of an Alloy 52 dissimilar metal weld. *Eng Fract Mech* 2019;214:320–34. <https://doi.org/10.1016/j.engfracmech.2019.03.001>.
- [30] Wallin K. Fracture toughness of engineering materials - estimation and application. EMAS publishing; 2011.
- [31] Wallin K, Laukkanen A, Nevasmaa P. Risk informed plant life management - application of the Master-Curve approach for hydrotreating reactors in an oil refinery. In: Solin J, editor. *Plant life Manag. - Prog. Struct. Integr. Espoo: VTT*; 2003.
- [32] Kocak M, Webster S, Janosch JJ, Ainsworth RA, Koers R, editors. FITNET - fitness for service - fracture, fatigue, creep, corrosion. 1st ed. Germany: 2008.